Available online at www.sciencedirect.com
SCIENCE DIRECT®
ELSEVIER
International Journal of Solids and Structures 42 (2005) 5692–5714
INTERNATIONAL JOURNAL OF SOLIDS and STRUCTURES
www.elsevier.com/locate/ijsolstr

An analytical and numerical approach for calculating effective material coefficients of piezoelectric fiber composites

Harald Berger [a,*], Sreedhar Kari [a], Ulrich Gabbert [a], Reinaldo Rodriguez-Ramos [b], Raul Guinovart [b], Jose A. Otero [b], Julian Bravo-Castillero [b]

[a] *Institute of Mechanics, Otto-von-Guericke-University of Magdeburg, Universitaetsplatz 2, D-39106 Magdeburg, Germany*
[b] *Facultad de Matemática y Computación, Universidad de la Habana, San Lázaro y L, CP 10400, Vedado, Habana 4, Cuba*

Received 28 October 2004
Available online 19 April 2005

Abstract

The present work deals with the modeling of 1–3 periodic composites made of piezoceramic (PZT) fibers embedded in a soft non-piezoelectric matrix (polymer). We especially focus on predicting the effective coefficients of periodic transversely isotropic piezoelectric fiber composites using representative volume element method (unit cell method). In this paper the focus is on square arrangements of cylindrical fibers in the composite. Two ways for calculating the effective coefficients are presented, an analytical and a numerical approach. The analytical solution is based on the asymptotic homogenization method (AHM) and for the numerical approach the finite element method (FEM) is used. Special attention is given on definition of appropriate boundary conditions for the unit cell to ensure periodicity. With the two introduced methods the effective coefficients were calculated for different fiber volume fractions. Finally the results are compared and discussed.

Keywords: Composite materials; Piezoelectric; Micromechanics; Homogenization; Finite element method

1. Introduction

Piezoelectric materials have the property of converting electrical energy into mechanical energy and vice versa. This reciprocity in the energy conversion makes piezoelectric ceramics such as PZT (lead zirconium

* Corresponding author. Tel.: +49 391 6712406; fax: +49 391 6712439.
E-mail address: harald.berger@mb.uni-magdeburg.de (H. Berger).

0020-7683/$ - see front matter © 2005 Elsevier Ltd. All rights reserved.
doi:10.1016/j.ijsolstr.2005.03.016

titanat) very attractive materials towards sensors and actuators applications. Even if their properties make them interesting, they are often limited, first by their weight, that can be a clear disadvantage for shape control and as a consequence, by their high specific acoustic impedance, which reduces their acoustic matching with the external fluid domain. Bulk piezoelectric materials have several drawbacks, hence composite materials are often a better technological solution in the case of a lot of applications such as ultrasonic transducers, medical imaging, sensors, actuators and damping. For the last 20 years, composite piezoelectric materials have been developed by combining piezoceramics with passive non-piezoelectric polymers. Superior properties have been achieved by these composites by taking advantage of most profitable properties of each constituents and a great variety of structures have been produced. Recently, due to the miniaturization of piezoelectric composites and the use of PZT fibers instead of piezoelectric bars, new applications toward electromechanical sensors and actuators have become possible. But, because the fibers are now much smaller than the wavelength, homogenization techniques are necessary to describe the behavior of piezoelectric composites.

Even if analytical and semi analytical models have been developed to homogenize piezoelectric composites, they are often reduced to specific cases. Numerical methods, such as the finite element method, seem to be a well-suited approach to describe the behavior of these materials, because there are no restrictions to the geometry, the material properties, the number of phases in the piezoelectric composite, and the size. However, finite element results are sensitive to mesh density. So it could be a difficult task to find appropriate meshes.

The prediction of the mechanical and electrical properties of piezoelectric fiber composites became an active research area in recent years. Except from experimental investigations, either micro- or macro mechanical methods are used to obtain the overall properties of piezoelectric fiber composites. Micro mechanical methods provide an overall behavior of piezoelectric fiber composites from known properties of their constituents (fiber and matrix) through an analysis of a periodic representative volume element (RVE) or a unit cell model. In the macro mechanical approach, on the other hand, the heterogeneous structure of the composite is replaced by a homogeneous medium with anisotropic properties. The advantage of the micro mechanical approach is that not only the global properties of the composites can be calculated, but also various mechanisms such as damage initiation and propagation, crack growth, etc. can be studied through the analysis.

A number of methods have been developed to predict and to simulate the coupled piezoelectric and mechanical behavior of composites. Basic analytical approaches have been reported (e.g. Chan and Unsworth, 1989; Smith and Auld, 1991), which are not capable of predicting the response to general loading, i.e. they do not give the full set of overall material parameters. Semi analytical and Hashin/Shtrikman-type bounds for describing the complete overall behavior (i.e. all elements of the material tensors) have been developed (Bisegna and Luciano, 1996, 1997) which are useful tools for theoretical considerations. However, the range between the bounds can be very wide for certain effective moduli. Mechanical mean field type methods have been extended to include electro-elastic effects (Benveniste, 1993; Dunn and Taya, 1993; Wang, 1992; Chen, 1993) based on an Eshelby-type solution for a single inclusion in an infinite matrix (Benveniste, 1992; Dunn and Wienecke, 1997). Such mean field type methods are capable of predicting the entire behavior under arbitrary loads. However, they use averaged representations of the electric and mechanical field within the constituents of the composite. This restriction can be overcome by employing periodic micro field approaches (commonly referred to as unit cell models) where the fields are typically solved numerically with high resolution, e.g. by the finite element method (Gaudenzi, 1997). In such models the representative unit cell and the boundary conditions are designed to capture a few special load cases, which are connected to specific deformation patterns (e.g. Brockenbrough and Suresh, 1990; Böhm, 1993; Gunawardena et al., 1993; Cleveringa et al., 1997). This allows the prediction of only a few key material parameters; for example, only normal loads can be applied consistently using the symmetry boundary conditions. A different method which can handle arbitrary loading scenarios is the

so-called asymptotic homogenization approach (Suquet, 1987; Bakhvalov and Panasenko, 1989). The local problems are considered and the effective elastic, piezoelectric and dielectric moduli are explicitly determined analytically.

Using the finite element method Poizat and Sester (1999) meshed the unit cell of the material and by applying specific boundary conditions, he has determined two piezoelectric coefficients. To the knowledge of the authors, the only unit cell models which capture the entire behavior correctly so far have been reported by Teply and Dvorak (1988) and recently by Smith et al. (1998). Presumably correct boundary conditions are employed in Reisner et al. (1998), Bisegna and Luciano (1997), although no details are given. The aim of this paper is to predict the full set of material moduli, i.e. to determine the complete tensors associated with the overall elastic, dielectric and piezoelectric behavior. This means that the linear response to any mechanical and electrical load, or any combination of both, will be determined. FEM tools have been extensively used in the literature to analyze a periodic unit cell, to determine the effective properties and damage mechanisms of piezoelectric fiber composites. In the present paper the FEM based micromechanical analysis method is applied to unidirectional periodic piezoelectric fiber composites subjected to different loading conditions with different boundary conditions to predict the effective coefficients of transversely isotropic piezoelectric fiber composites (1–3 periodic).

The effective coefficients are predicted for various fiber volume fractions by using the asymptotic homogenization method on one hand (analytical solution) and on the other hand by means of finite element method (numerical solution). Both results are compared and discussed.

2. Piezoelectricity and piezoelectric composites

Coupled piezoelectric problems are those in which an electric potential gradient causes deformation (converse piezoelectric effect), while mechanical strains cause an electric potential gradient in the material (direct piezoelectric effect). The coupling between mechanical and electric fields is characterized by piezoelectric coefficients. Those materials respond linearly to changes in the electric field, the electrical displacements, or mechanical stresses and strains. These assumptions are compatible with the piezoelectric ceramics, polymers, and composites in current use (Silva et al., 1998). Therefore, the behavior of the piezoelectric medium is described by the following piezoelectric constitutive equations, which correlate stresses (T_{ij}), strains (S_{kl}), electric fields (E_k), and electrical displacements (D_i) as follows:

$$\begin{aligned} T_{ij} &= C_{ijkl}S_{kl} - e_{kij}E_k, \\ D_i &= e_{ikl}S_{kl} + \varepsilon_{ik}E_k, \end{aligned} \tag{1}$$

where C_{ijkl} is the fourth-order elasticity tensor under short circuit boundary conditions, ε_{ik} is the second-order free body electric tensor, and e_{kij} is the third-order piezoelectric strain tensor. Due to the symmetry of the tensors T_{ij}, S_{ij}, C_{ijkl}, and ε_{ij}, the above Eq. (1) can be written in a vector/matrix notation by using Voigt's notation as

$$\begin{bmatrix} T \\ D \end{bmatrix} = \begin{bmatrix} C & -e^{\mathrm{T}} \\ e & \varepsilon \end{bmatrix} \begin{bmatrix} S \\ E \end{bmatrix}, \tag{2}$$

where superscript T denotes a transposed matrix.

For a transversely isotropic piezoelectric solid, the stiffness matrix, the piezoelectric matrix and the dielectric matrix simplify so that there remain 11 independent coefficients. In the case of aligned fibers made of a transversely isotropic piezoelectric solid (PZT), embedded in an isotropic polymer matrix, the resulting composite is a transversely isotropic piezoelectric material too. Consequently, the constitutive Eq. (2) can be written as

$$\begin{bmatrix} \overline{T}_{11} \\ \overline{T}_{22} \\ \overline{T}_{33} \\ \overline{T}_{23} \\ \overline{T}_{31} \\ \overline{T}_{12} \\ \overline{D}_1 \\ \overline{D}_2 \\ \overline{D}_3 \end{bmatrix} = \begin{bmatrix} C_{11}^{\text{eff}} & C_{12}^{\text{eff}} & C_{13}^{\text{eff}} & 0 & 0 & 0 & 0 & 0 & -e_{13}^{\text{eff}} \\ C_{12}^{\text{eff}} & C_{11}^{\text{eff}} & C_{13}^{\text{eff}} & 0 & 0 & 0 & 0 & 0 & -e_{13}^{\text{eff}} \\ C_{13}^{\text{eff}} & C_{13}^{\text{eff}} & C_{33}^{\text{eff}} & 0 & 0 & 0 & 0 & 0 & -e_{33}^{\text{eff}} \\ 0 & 0 & 0 & C_{44}^{\text{eff}} & 0 & 0 & 0 & -e_{15}^{\text{eff}} & 0 \\ 0 & 0 & 0 & 0 & C_{44}^{\text{eff}} & 0 & -e_{15}^{\text{eff}} & 0 & 0 \\ 0 & 0 & 0 & 0 & 0 & C_{66}^{\text{eff}} & 0 & 0 & 0 \\ 0 & 0 & 0 & 0 & e_{15}^{\text{eff}} & 0 & \varepsilon_{11}^{\text{eff}} & 0 & 0 \\ 0 & 0 & 0 & e_{15}^{\text{eff}} & 0 & 0 & 0 & \varepsilon_{11}^{\text{eff}} & 0 \\ e_{13}^{\text{eff}} & e_{13}^{\text{eff}} & e_{33}^{\text{eff}} & 0 & 0 & 0 & 0 & 0 & \varepsilon_{33}^{\text{eff}} \end{bmatrix} \begin{bmatrix} \overline{S}_{11} \\ \overline{S}_{22} \\ \overline{S}_{33} \\ \overline{S}_{23} \\ \overline{S}_{31} \\ \overline{S}_{12} \\ \overline{E}_1 \\ \overline{E}_2 \\ \overline{E}_3 \end{bmatrix}. \tag{3}$$

In this matrix the general variables of the coupled electromechanical problem were replaced by the appropriate values for the homogenized structure. So, C_{ij}^{eff}, e_{ij}^{eff}, $\varepsilon_{ij}^{\text{eff}}$ denote the effective material coefficients and $\overline{S}_{ij}$, $\overline{E}_i$, $\overline{T}_{ij}$, $\overline{D}_i$ denote average values. These relations represent the basis for the further considerations based on the unit cell.

3. Representative volume element (unit cell) method

In general the object under consideration is regarded as a large-scale/macroscopic structure. The common approach to model the macroscopic properties of 3D piezoelectric fiber composites is to create a representative volume element (RVE) or a unit cell that captures the major features of the underlying microstructure. The mechanical and physical properties of the constituent material is always regarded as a small-scale/micro structure. One of the most powerful tools to speed up the modeling process, both the composite discretization and the computer simulation of composites in real conditions, is the homogenization method. The main idea of the method is to find a globally homogeneous medium equivalent to the original composite, where the strain energy stored in both systems is approximately the same. Different analytical homogenization techniques have been developed in order to predict the effective properties of piezoelectric composites. Uni-directional (1–3 periodic) piezoelectric fiber composites can be analyzed by using asymptotic homogenization method. Inclusion problems (i.e. 0–3 periodic) can be analyzed by self-consistent methods (see Levin et al., 1999). Moreover, numerical methods (e.g. FEM techniques) have been developed to evaluate the effective coefficients of composites. In this paper we limit ourselves to a quasistatic analysis of periodic (1–3) structures with perfectly bonded continuous fibers which are aligned and poled

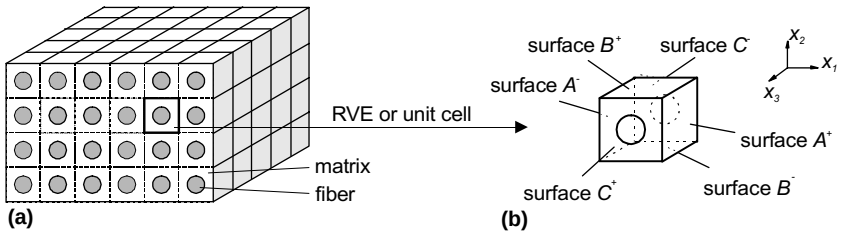

Fig. 1. Schematic diagram of a periodic 1–3 composite: (a) and unit cell, (b) picked from the original composite.

along the x_3 axis as shown in Fig. 1. With help of symmetry, such a regular piezoelectric fiber composite may be analyzed by using a representative volume element or unit cell. A unit cell is the smallest part that contains sufficient information on the above-mentioned geometrical and material parameters at the microscopic level to deduce the effective properties of the composite.

Fig. 1 shows the unit cell that is picked from the periodic piezoelectric fiber composite. It has infinite lengths in all three directions. In this paper we consider a composite with a square fiber arrangement. It is assumed that the material properties are the same in the first two directions (i.e. along x_1 and x_2 axis). All the fibers are assumed to be straight and poled in the third direction (i.e. along axis x_3). Fig. 1(b) shows the schematic diagram of the unit cell picked from the considered composite.

4. Analytical solution using asymptotic homogenization method

For a heterogeneous and periodic medium Ω' the constitutive relations of the linear piezoelectricity theory in Eq. (1) are characterized by different material coefficients: C (elastic), e (piezoelectric) and ε (dielectric) which are X periodic functions. X denotes the periodic cell. By means of the asymptotic homogenization method (Bensoussan et al., 1978; Bravo-Castillero et al., 2001) the original constitutive relations (Eq. (1)) with rapidly oscillating material coefficients are transformed in two sets of mathematical problems.

The first set has new physical relations over Ω with constant coefficients: C^{eff} (elastic), e^{eff} (piezoelectric) and ε^{eff} (dielectric) which represent the properties of an equivalent homogeneous medium Ω and they are called the effective coefficients of the composite under study. They are calculated by using the following formulae (see Bravo-Castillero et al., 2001):

$$\begin{aligned} C^{\text{eff}}_{ijpq} &= \left\langle C_{ijpq}(x) + C_{ijkl}(x)\,{}_{pq}M_{k,l}(x) + e_{kij}(x)\,{}_{pq}N_{,k}(x)\right\rangle, \\ e^{\text{eff}}_{ipq} &= \left\langle e_{ipq}(x) + e_{ikl}(x)\,{}_{pq}M_{k,l}(x) - \varepsilon_{ik}(x)\,{}_{pq}N_{,k}(x)\right\rangle, \\ \varepsilon^{\text{eff}}_{ip} &= \left\langle \varepsilon_{ip}(x) - e_{ikl}(x)\,{}_{p}Q_{,k}(x) + \varepsilon_{ik}(x)\,{}_{p}P_{k,l}(x)\right\rangle, \end{aligned} \tag{4}$$

where $\langle f\rangle = \frac{1}{|X|}\int_X f\,\mathrm{d}X$. The material coefficients $C_{ijpq}(x)$, $e_{ipq}(x)$, $\varepsilon_{im}(x)$ are known functions of the constituents composite phases. $x = (x_1, x_2, x_3)$ is the local variable on the periodic cell X. The subscripts assume the values 1, 2 and 3; the comma denotes partial differentiation, and the summation convention is applied.

The second set allows the calculation of the functions ${}_{pq}M$, ${}_{pq}N$ and ${}_{p}P$ which are solutions of the so-called local problems ${}_{pq}L$ and ${}_{p}L$. The local problems ${}_{pq}L$ and ${}_{p}L$ are solved over the periodic cell X and they were derived in Bravo-Castillero et al., 2001. More precisely, this is given as follows.

We consider a two-phase fiber-reinforced piezoelectric composite body with x_3 as fiber direction and with a unit length parallel to the cylindrical fibers (see Fig. 1(b)). The composite constituents are homogeneous linear transversely isotropic piezoelectric materials, with the axis of transverse isotropy oriented in the direction of the fibers. The cell X of the body is chosen with a side parallel to x_3 and with unit length. The common interface between the fiber and the matrix is denoted by Γ.

The local problem ${}_{pq}L$ where the subscripts $p, q = 1, 2, 3$ and $pq = qp$, seeks the pq-displacement ${}_{pq}M^{(\alpha)}$ and the pq-potential ${}_{pq}N^{(\alpha)}$ in X_α, which are double periodic functions of periods $\omega_1 = (1, 0)$ and $\omega_2 = (0, 1)$ in the x_1 and x_2 directions, respectively. They are the solutions of

$$\begin{aligned} &{}_{pq}T^{(\alpha)}_{i\delta,\delta} = 0 \quad \text{in } X_\alpha; \qquad {}_{pq}D^{(\alpha)}_{\delta,\delta} = 0 \quad \text{in } X_\alpha; \\ &\|{}_{pq}M_i\| = 0 \quad \text{on } \Gamma; \qquad \|{}_{pq}N_i\| = 0 \quad \text{on } \Gamma; \\ &\|{}_{pq}T_{i\delta}n_\delta\| = -\|C_{i\delta pq}\|n_\delta \quad \text{on } \Gamma; \qquad \|{}_{pq}D_\delta n_\delta\| = -\|e_{\delta pq}\|n_\delta \quad \text{on } \Gamma; \\ &\langle {}_{pq}M_i\rangle = 0; \qquad \langle {}_{pq}N_i\rangle = 0, \end{aligned}$$

where

$$ {}_{pq}T^{(\alpha)}_{i\delta} = C^{(\alpha)}_{i\delta k\lambda}\,{}_{pq}M^{(\alpha)}_{k,\lambda} + e^{(\alpha)}_{\lambda i\delta}\,{}_{pq}N^{(\alpha)}_{,\lambda}; \qquad {}_{pq}D^{(\alpha)}_{\delta} = e^{(\alpha)}_{\delta k\lambda}\,{}_{pq}M^{(\alpha)}_{k,\lambda} - \varepsilon^{(\alpha)}_{\delta\lambda}\,{}_{pq}N^{(\alpha)}_{,\lambda}; $$
$$ {}_{pq}T^{(\alpha)}_{33} = C^{(\alpha)}_{3311}\,{}_{pq}M^{(\alpha)}_{\alpha,\alpha}; \qquad {}_{pq}D^{(\alpha)}_{3} = e^{(\alpha)}_{311}\,{}_{pq}M^{(\alpha)}_{\alpha,\alpha} $$

and

$$ {}_{pq}T^{(\alpha)}_{i\delta} = C^{(\alpha)}_{i\delta k\lambda pq}S^{(\alpha)}_{k,\lambda}; $$

the comma notation denotes a partial derivative with respect to the x_δ component; again the summation convention is applied, but it is taken over repeated lower cases indices only. X_α is the region occupied by the phase α. The outward unit normal vector to the interface Γ is n. The double bar notation $\|f\|$ denotes the jump of the function f across the interface Γ, i.e. $\|f\| = f^{(1)} - f^{(2)}$ whereas the indices (1) and (2) denotes the matrix and the fiber properties, respectively.

The ${}_pL$ problem is stated as follows: the p-displacement ${}_pP^{(\alpha)}$ and the p-potential ${}_pQ^{(\alpha)}$ are sought in X_α, which are periodic functions of periods $\omega_1 = (1,0)$ and $\omega_2 = (0,1)$ that satisfy the boundary-value problems

$$ {}_pT^{(\alpha)}_{i\delta,\delta} = 0 \quad \text{in } X_\alpha; \qquad {}_pD^{(\alpha)}_{\delta,\delta} = 0 \quad \text{in } X_\alpha; $$
$$ \left\|{}_{pq}P_i\right\| = 0 \quad \text{on } \Gamma; \qquad \left\|{}_{pq}Q_i\right\| = 0 \quad \text{on } \Gamma; $$
$$ \left\|{}_pT_{i\delta}n_\delta\right\| = -\left\|e_{pi\delta}\right\|n_\delta \quad \text{on } \Gamma; \qquad \left\|{}_pD_\delta n_\delta\right\| = -\left\|\varepsilon_{\delta p}\right\|n_\delta \quad \text{on } \Gamma; $$
$$ \left\langle {}_pP_i\right\rangle = 0; \qquad \left\langle {}_pQ_i\right\rangle = 0, $$

where

$$ {}_pT^{(\alpha)}_{i\delta} = C^{(\alpha)}_{i\delta k\lambda}\,{}_pP^{(\alpha)}_{k,\lambda} + e^{(\alpha)}_{\lambda i\delta}\,{}_pQ^{(\alpha)}_{,\lambda}; \qquad {}_pD^{(\alpha)}_{\delta} = e^{(\alpha)}_{\delta k\lambda}\,{}_pP^{(\alpha)}_{k,\lambda} - \varepsilon^{(\alpha)}_{\delta\lambda}\,{}_pQ^{(\alpha)}_{,\lambda}; $$
$$ {}_pT^{(\alpha)}_{33} = C^{(\alpha)}_{3311}\,{}_pP^{(\alpha)}_{\alpha,\alpha}; \qquad {}_pD^{(\alpha)}_{3} = e^{(\alpha)}_{311}\,{}_pP^{(\alpha)}_{\alpha,\alpha}. $$

The analytical solution of the local problems, which is based upon the complex-potential method of Muskhelishvili, utilizes a series expansion of the doubly periodic Weierstrass elliptic functions to predict both the local and overall averaging properties of the composite materials (Pobedria, 1984; Meguid and Kalamkarov, 1994).

Using Eq. (4) we obtain for the plane-problem the following expressions for the global properties of the composite:

$$ \begin{aligned} &\bar{k} = k_{\mathrm{v}} - V_2\|k\|^2K/m_1, \quad \bar{l} = l_{\mathrm{v}} - V_2\|l\|\|k\|K/m_1, \quad \bar{n} = n_{\mathrm{v}} - V_2\|l\|^2K/m_1, \\ &\bar{m} = m_{\mathrm{v}} - V_2\|m\|M, \quad \bar{m}' = m_{\mathrm{v}} - V_2\|m\|M', \quad \bar{q} = q_{\mathrm{v}} - V_2\|q\|\|k\|K/m_1, \\ &\bar{r} = r_{\mathrm{v}} - V_2\|l\|\|q\|K/m_1, \quad \bar{u} = u_{\mathrm{v}} + V_2\|q\|^2K/m_1. \end{aligned} \tag{5} $$

In the above equations the coefficients $k = (C_{1111} + C_{1122})/2$, $l = C_{1133} = C_{2233}$, $m' = (C_{1111} - C_{1122})/2$, $m = C_{1212}$ and $n = C_{3333}$, correspond to elasticity. The coefficients $q = e_{311} = e_{322}$ and $r = e_{333}$ are piezoelectric ones, and $u = \varepsilon_{33}$ is a dielectric constant. The subscripts v refer to the Voigt average of the relevant quantity, i.e. the phase-mixing rule in the cross section of the composite. For instance, $k_{\mathrm{v}} = k_1V_1 + k_2V_2$, etc., and V_α are the area fractions occupied by the matrix and fiber materials, respectively, and $V_1 + V_2 = 1$. The constants K, M and M' are calculated according to the expressions (3.36) and (3.38b) on pp. 231–232 in Rodriguez-Ramos et al. (2001) and the rest of effective properties $p = C_{1313}$, $s = e_{113}$ and $t = \varepsilon_{11}$ related to the anti-plane problem ${}_{13}L$ are computed following the formulae (3.26) on pp. 244 in Bravo-Castillero, et al. (2001).

5. Numerical solution using finite element method

5.1. Periodic boundary conditions to RVE

Composite materials can be represented as a periodical array of RVEs. Therefore, periodic boundary conditions must be applied to the RVE models. This implies that each RVE in the composite has the same deformation mode and there is no separation or overlap between the neighboring RVEs. These periodic boundary conditions on the boundary RVE are given by Suquet (1987)

$$u_i = \overline{S}_{ij} x_j + v_i. \tag{6}$$

In the above Eq. (6) $\overline{S}_{ij}$ are the average strains, v_i is the periodic part of the displacement components (local fluctuation) on the boundary surfaces, which is generally unknown and is dependent on the applied global loads. The indices i and j denote the global three-dimensional coordinate directions in the range from 1 to 3. A more explicit form of periodic boundary conditions, suitable for square RVE models can be derived from the above general expression. For the RVE as shown in Fig. 1(b), the displacements on a pair of opposite boundary surfaces (with their normal along the x_j axis) are

$$u_i^{K^+} = \overline{S}_{ij} x_j^{K^+} + v_i^{K^+}, \tag{7}$$

$$u_i^{K^-} = \overline{S}_{ij} x_j^{K^-} + v_i^{K^-}, \tag{8}$$

where index 'K^+' means along the positive x_j direction and 'K^-' means along the negative x_j direction on the corresponding surfaces A^-/A^+, B^-/B^+ and C^-/C^+ (see Fig. 1(b)). The local fluctuations $v_i^{K^+}$ and $v_i^{K^-}$ around the average macroscopic value are identical on two opposing faces due to periodic conditions of RVE. So, the difference between the above two equations is the applied macroscopic strain condition

$$u_i^{K^+} - u_i^{K^-} = \overline{S}_{ij}\left(x_j^{K^+} - x_j^{K^-}\right). \tag{9}$$

Similarly the periodic boundary condition for electric potential is given by the applied macroscopic electric field condition and is

$$\Phi^{K^+} - \Phi^{K^-} = \overline{E}_i\left(x_j^{K^+} - x_j^{K^-}\right). \tag{10}$$

It is assumed that the average mechanical and electrical properties of a RVE are equal to the average properties of the particular composite. The average stresses and strains in a RVE are defined by

$$\overline{S}_{ij} = \frac{1}{V}\int_V S_{ij}\,\mathrm{d}V, \tag{11}$$

$$\overline{T}_{ij} = \frac{1}{V}\int_V T_{ij}\,\mathrm{d}V, \tag{12}$$

where V is the volume of the periodic representative volume element. Analogous the average electric fields and electrical displacements are defined by

$$\overline{E}_i = \frac{1}{V}\int_V E_i\,\mathrm{d}V, \tag{13}$$

$$\overline{D}_i = \frac{1}{V}\int_V D_i\,\mathrm{d}V. \tag{14}$$

5.2. Finite element modeling

All finite element calculations were made with FE package ANSYS. For modeling the RVE three-dimensional multi-field 8 node brick elements with displacement degrees of freedom (DOF) and additional electric potential (voltage) degree of freedom were used. These allows for fully coupled electromechanical analyses.

To obtain the homogenized effective properties we apply the macroscopic boundary conditions (Eqs. (9) and (10)) to the RVE by coupling opposite nodes on opposite boundaries. In order to apply these periodic boundary conditions in the FE analysis, the mesh on the opposite boundary surfaces must be the same. For each pair of displacement components at two corresponding nodes with identical in-plane coordinates on the two opposite boundary surfaces a constraint condition (periodic boundary condition Eq. (9) or (10)) is imposed. The prescription of these constraint conditions to all opposite nodes at opposite boundary surfaces directly in ANSYS is a very difficult task because of too many number of nodes. Consequently, we developed a FORTRAN program which generates all required constraint conditions automatically. First the finite element mesh is created from the ANSYS preprocessor. Then based on the generated nodal coordinates the appropriate nodal pairs are selected by the FORTRAN program and a partial ANSYS input file is created containing the constraint conditions. Using this input file ANSYS continues with assigning the constraint equations and finally with solving the problem. As an example Fig. 2 shows the constraint equations for a pair of nodes on opposite surfaces A^- and A^+.

For the calculation of effective coefficients we consider a piezoceramic (PZT-5) fiber embedded in a soft non-piezoelectric material (polymer). In analytical as well as in numerical modeling, we are assuming that the fibers and the matrix are ideally bonded and that the fibers are straight and parallel to the x_3 axis. The fiber section is circular and the unit cell is having a square cross section. The piezoelectric fibers are uniformly poled along the x_3 direction. The material properties of polymer and PZT-5 are listed in Table 1, where elastic properties, piezoelectric constants and permittivities are given in N/m^2, C/m^2 and F/m, respectively.

To find the effective coefficients special load cases with different boundary conditions must be constructed in such a way that for a particular load case only one value in the strain/electric field vector (see Eq. (3)) is non-zero and all others become zero. Then from one row in Eq. (3) the corresponding effective coefficient can be calculated using the calculated average non-zero value in the strain/electric field vector and the calculated average values in the stress/electrical displacement vector.

In the next chapters the special models for calculating different effective coefficients are explained in detail. Every load case was calculated for six different fiber volume fractions in the range from 0.111 to 0.666

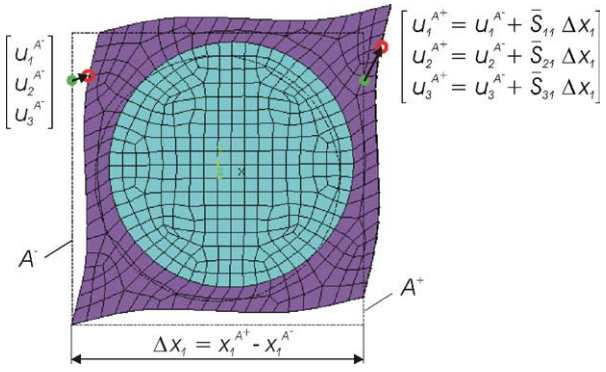

Fig. 2. Periodic boundary conditions for a pair of nodes on opposite surfaces A^- and A^+.

Table 1
Material properties of the composite constituents fiber (PZT-5) and matrix (polymer)

	C_{11} (10^{10})	C_{12} (10^{10})	C_{13} (10^{10})	C_{33} (10^{10})	C_{44} (10^{10})	C_{66} (10^{10})	e_{15}	e_{13}	e_{33}	ε_{11} (10^{-9})	ε_{33} (10^{-9})
PZT-5	12.1	7.54	7.52	11.1	2.11	2.28	12.3	−5.4	15.8	8.11	7.35
Polymer	0.386	0.257	0.257	0.386	0.064	0.064	–	–	–	0.07965	0.07965

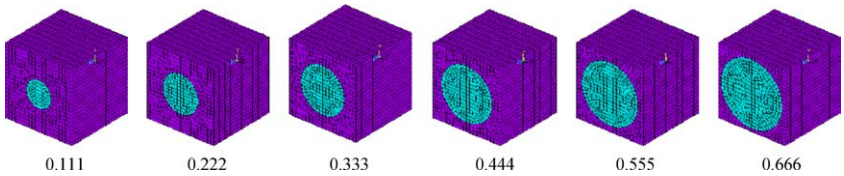

Fig. 3. Investigated ratios of fiber volume fraction.

with steps of 0.111. Fig. 3 visualizes the relation of fiber and matrix for the different investigated fractions. Since only the volume fiber fraction has an influence on the results the size of the RVE was chosen as a unit length.

6. Numerical calculation of the different effective coefficients

6.1. Calculation of C_{13}^{eff} and C_{33}^{eff}

For the calculation of the effective coefficients C_{13}^{eff} and C_{33}^{eff} the boundary conditions have to be applied to the RVE in such a way that, except the strain in the x_3 direction ($\overline{S}_{33}$), all other mechanical strains and gradients of electric potential ($\overline{E}_i$) become zero. This can be achieved by constraining the normal displacements at all surfaces to zero except of surface C^+ (see Fig. 1(b)). At surface C^+ the periodic boundary condition corresponding to surface C^- must be applied. Due to applied zero displacements to surface C^- in x_3 direction ($u_3^{C^-} = 0$) the periodic boundary condition in this direction according to Eq. (9) simplifies to

$$u_3^{K^+} = \overline{S}_{33}\left(x_3^{K^+} - x_3^{K^-}\right). \tag{15}$$

Because now this equation is independent of $u_3^{C^-}$, instead of using constraint equations, an arbitrary constant prescribed displacement can be applied on surface C^+ to produce a strain in x_3 direction.

To make gradients of the electric potential in all directions zero the voltage degree of freedom on all surfaces is set to zero.

Fig. 4 shows the finite element mesh. In Figs. 5 and 6 the distribution of the strain S_{33} and the stress T_{33} is shown in the deformed model, respectively.

For the calculation of the total average values $\overline{S}_{33}$, $\overline{T}_{11}$ and $\overline{T}_{33}$ according to Eqs. (11) and (12) the integral was replaced by a sum over averaged element values multiplied by the respective element volume. Using these total average values the coefficients C_{13}^{eff} and C_{33}^{eff} can be calculated from the matrix Eq. (3). Due to zero strains and electric fields, except $\overline{S}_{33}$ the first row becomes $\overline{T}_{11} = C_{13}^{\text{eff}}\overline{S}_{33}$. Then C_{13}^{eff} can be calculated as the ratio of $\overline{T}_{11}/\overline{S}_{33}$. Similarly C_{33}^{eff} can be evaluated as the ratio of $\overline{T}_{33}/\overline{S}_{33}$ from the third row of matrix Eq. (3).

Figs. 7 and 8 show the variation of these effective coefficients for different volume fractions in comparison to the calculated values by AHM.

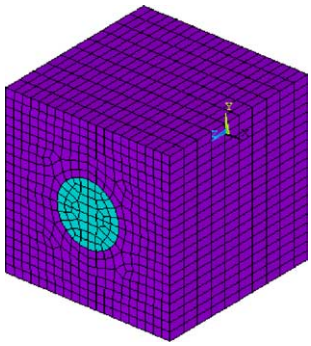

Fig. 4. Finite element mesh.

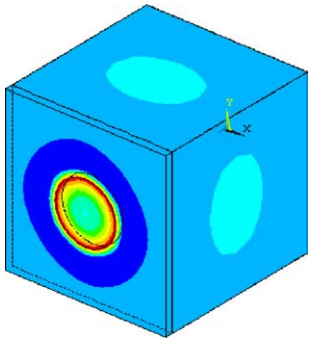

Fig. 5. Strain distribution S_{33}.

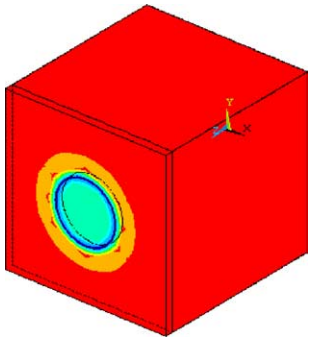

Fig. 6. Stress distribution T_{33}.

6.2. Calculation of C_{11}^{eff} and C_{12}^{eff}

For the calculation of the effective coefficients C_{11}^{eff} and C_{12}^{eff} we have similar conditions like for the calculation of the effective coefficients C_{13}^{eff} and C_{33}^{eff}. But now a prescribed displacement in x_1 direction must be applied on surface A^+ and the normal displacements on all other surfaces must be set to zero. Also the

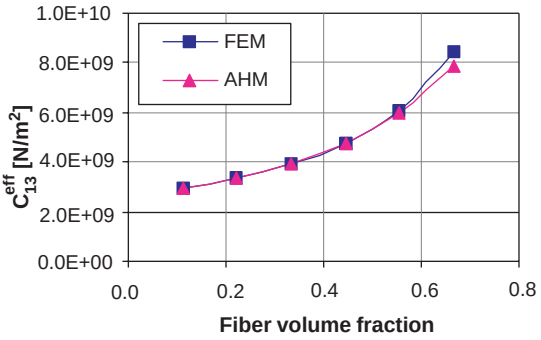

Fig. 7. Variation of C_{13}^{eff} as a function of volume fraction and comparison between FEM and AHM.

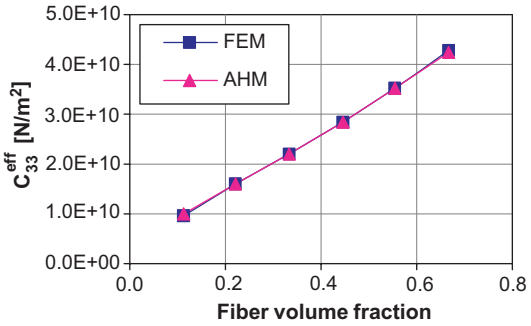

Fig. 8. Variation of C_{33}^{eff} as a function of volume fraction and comparison between FEM and AHM.

electric potential DOF at all surfaces is set to zero. For the calculation of these coefficients the in-plane behavior is relevant only. That's why modeling of a small slice with one element in x_3 direction is sufficient. Fig. 9 shows this model including the finite element mesh. The calculated distribution of the strains S_{11} and stresses T_{11} are shown in the deformed configuration in Figs. 10 and 11, respectively.

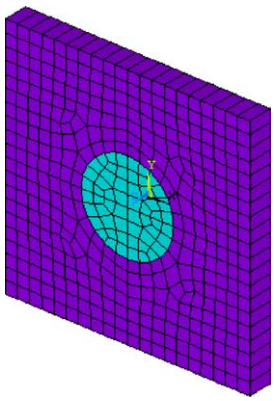

Fig. 9. Finite element mesh.

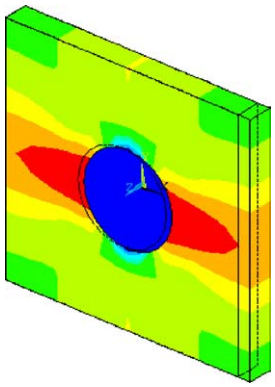

Fig. 10. Strain distribution S_{11}.

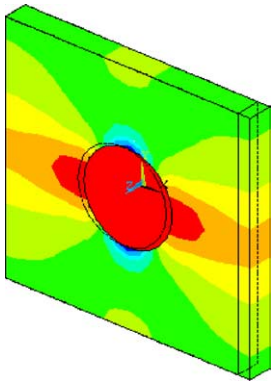

Fig. 11. Stress distribution T_{11}.

Using the total average strain $\overline{S}_{11}$ and stress $\overline{T}_{11}$ from first row of matrix Eq. (3) we get $\overline{T}_{11} = C_{11}^{\text{eff}}\overline{S}_{11}$. From this relation C_{11}^{eff} can be calculated as the ratio of $\overline{T}_{11}/\overline{S}_{11}$. Similarly C_{12}^{eff} can be found as the ratio of $\overline{T}_{22}/\overline{S}_{11}$ using the second row of matrix Eq. (3). Figs. 12 and 13 show the variation of these effective coefficients for different volume fractions in comparison with the calculated values by AHM.

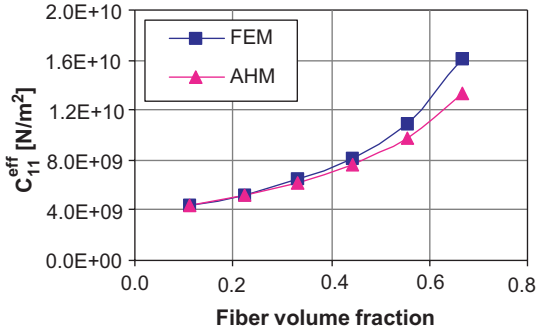

Fig. 12. Variation of C_{11}^{eff} as a function of volume fraction and comparison between FEM and AHM.

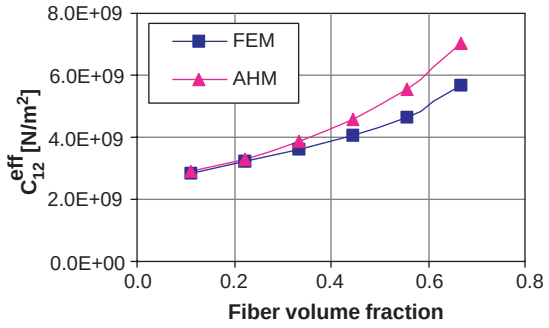

Fig. 13. Variation of C_{12}^{eff} as a function of volume fraction and comparison between FEM and AHM.

6.3. Calculation of C_{66}^{eff} and C_{44}^{eff}

To evaluate the effective coefficient C_{66}^{eff} the in-plane shear strain $\overline{S}_{12}$ may have a non-zero value in strain/electric field vector of Eq. (3) only. For the evaluation of C_{44}^{eff} the out-of-plane shear strain $\overline{S}_{23}$ or $\overline{S}_{31}$ may have a non-zero value only. This can be achieved by applying appropriate shear forces to produce a pure shear stress state in the desired directions which, consequently, results in a pure shear strain state. Beside the applied shear forces the displacement boundary conditions must be chosen in the right way to get these states. That means that a symmetric deformation mode respective to the diagonal line of the shear plane must be ensured; see also Fig. 2, which visualizes such a pure shear stress state in a plane view. To receive such pure shear stress state a support normal to the diagonal at one edge of the finite element model was applied. To avoid rigid body movement the opposite edge was fixed in the shear plane. Figs. 14 and 17 show these finite element models with shear forces and the above mentioned supports for both load cases, respectively. For the calculation of C_{44}^{eff} the x_2–x_3 plane was chosen as shear plane. Furthermore normal displacements at parallel surfaces to the shear plane must be set to zero to ensure zero strains perpendicular to the shear plane. Also the electric potential DOF on all surfaces must be set to zero. The calculated stress and strain distribution is shown in Figs. 15, 16 and 18, 19.

Using the calculated non-zero average strain and stress values from the first model the sixth row in the matrix Eq. (3) becomes $\overline{T}_{12} = C_{66}^{\text{eff}}\overline{S}_{12}$ and, consequently, C_{66}^{eff} can be evaluated as the ratio of $\overline{T}_{12}/\overline{S}_{12}$. With

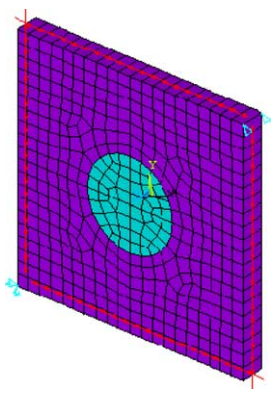

Fig. 14. Finite element mesh with shear loads and in-plane supports.

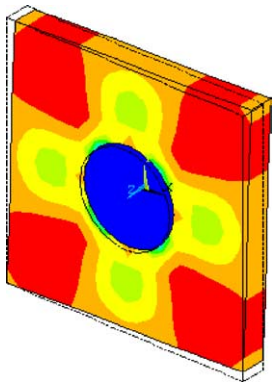

Fig. 15. Strain distribution S_{12}.

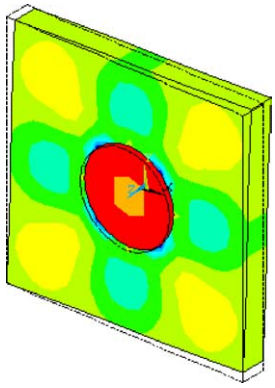

Fig. 16. Stress distribution T_{12}.

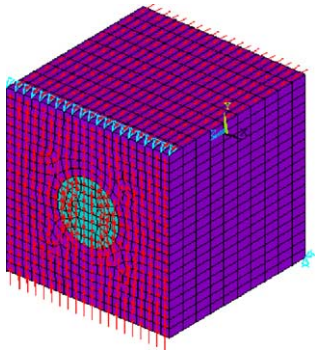

Fig. 17. Finite element mesh with shear loads and out-of-plane supports.

the second model C_{44}^{eff} can be found as the ratio of $\overline{T}_{23}/\overline{S}_{23}$. Figs. 20 and 21 show the variation of these effective coefficients for different volume fractions.

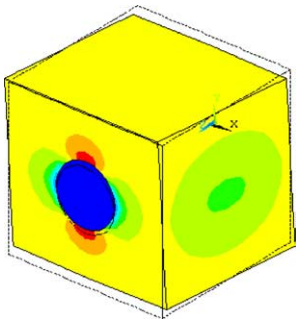

Fig. 18. Strain distribution S_{23}.

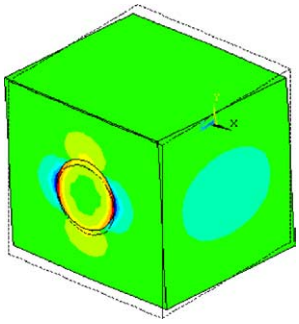

Fig. 19. Stress distribution T_{23}.

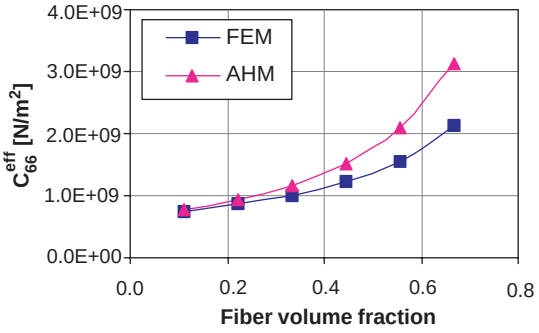

Fig. 20. Variation of C_{66}^{eff} as a function of volume fraction and comparison between FEM and AHM.

6.4. Calculation of e_{13}^{eff}, e_{33}^{eff} and ε_{33}^{eff}

In order to evaluate the effective coefficients e_{13}^{eff}, e_{33}^{eff} and $\varepsilon_{33}^{\text{eff}}$, all surfaces must be constrained to have zero normal displacements. A zero electric potential is applied to the surface C^- and a non-zero electric potential is applied to the surface C^+. The electric potential at all other surfaces is set to zero. Since all surfaces are constrained to have zero displacements and because of the electric potential difference in x_3 direction the fiber will try to expand and stresses as well as electric fields are produced in x_3 direction. The calculated distribution of T_{33}, T_{11} and D_3 is shown in Figs. 22–24.

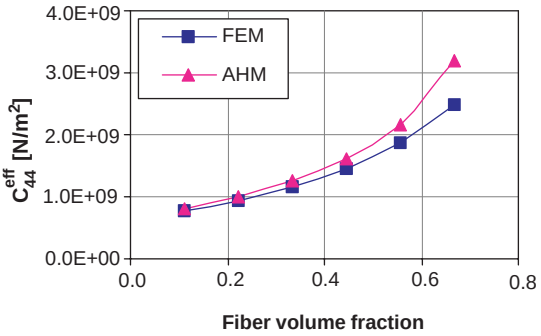

Fig. 21. Variation of C_{44}^{eff} as a function of volume fraction and comparison between FEM and AHM.

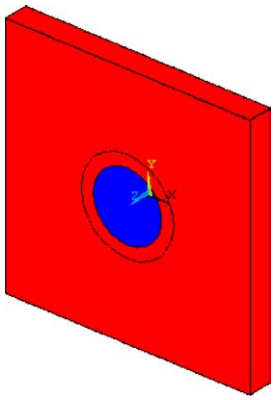

Fig. 22. Stress distribution T_{33}.

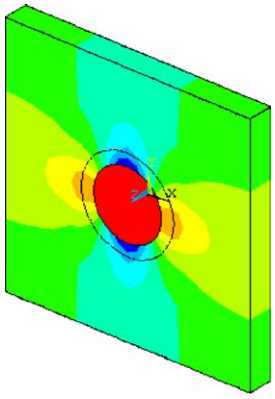

Fig. 23. Stress distribution T_{11}.

Consequently, the total average stress and electrical displacement values as well as the total average electric field $\overline{E}_3$ can be calculated. Then the third row of the matrix Eq. (3) reduces to $\overline{T}_{33} = -e_{33}^{\text{eff}}\overline{E}_3$, so that $e_{33}^{\text{eff}} = -\overline{T}_{33}/\overline{E}_3$. Similarly e_{13}^{eff} is the ratio of $-\overline{T}_{11}/\overline{E}_3$. For the evaluation of $\varepsilon_{33}^{\text{eff}}$ the last row of matrix

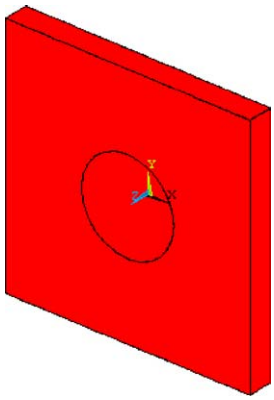

Fig. 24. Electrical displacement distribution D_3.

Eq. (3) is used which becomes $\overline{D}_3 = \varepsilon_{33}^{\text{eff}}\overline{E}_3$. From this equation $\varepsilon_{33}^{\text{eff}}$ can be calculated by $\varepsilon_{33}^{\text{eff}} = -\overline{D}_3/\overline{E}_3$. Figs. 25–27 show the variation of these effective coefficients for different volume fractions.

6.5. Calculation of e_{15}^{eff}

The effective coefficient e_{15}^{eff} can be calculated as the ratio of $\overline{D}_2/\overline{S}_{23}$ from the seventh row of the matrix. In order to evaluate this coefficient, the boundary conditions should be applied in such a way that except of

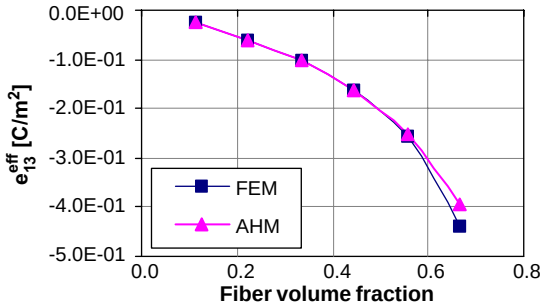

Fig. 25. Variation of e_{13}^{eff} as a function of volume fraction and comparison between FEM and AHM.

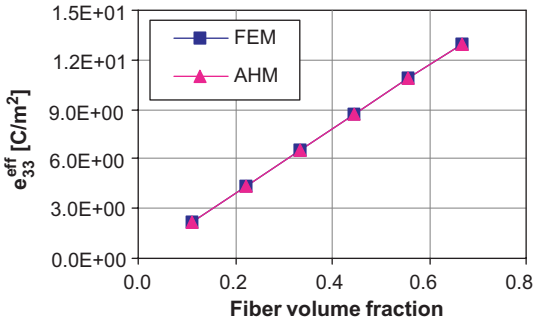

Fig. 26. Variation of e_{33}^{eff} as a function of volume fraction and comparison between FEM and AHM.

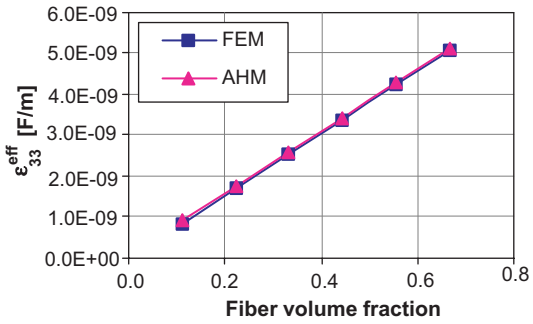

Fig. 27. Variation of $\varepsilon_{33}^{\text{eff}}$ as a function of volume fraction and comparison between FEM and AHM.

the strain $\overline{S}_{23}$ in the strain/electric field vector in Eq. (3), all other strains and electric fields are made to zero. Similarly to the calculation of C_{44}^{eff} out-of-plane shear forces are applied in the x_2–x_3 plane (Fig. 28). The electric potential in all directions is made to zero by constraining the voltage degree of freedom to zero. Consequently, in the matrix Eq. (3) the eighth row becomes $\overline{D}_2 = e_{15}^{\text{eff}}\overline{S}_{23}$. From this equation e_{15}^{eff} can be calculated by the ratio $e_{15}^{\text{eff}} = \overline{D}_2/\overline{S}_{23}$. The calculated distribution of S_{23} and D_2 is shown in Figs. 29 and 30. Fig. 31 shows the variation of this effective coefficients for different volume fractions in comparison with the calculated values by AHM.

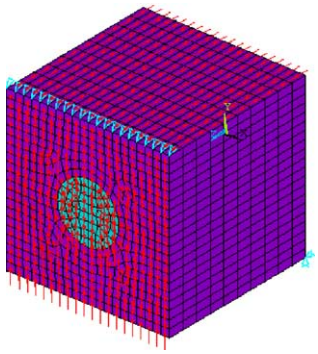

Fig. 28. Finite element mesh with shear loads and out-of-plane supports.

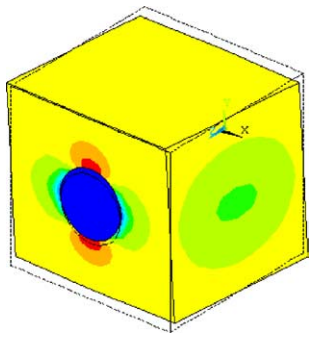

Fig. 29. Strain distribution S_{23}.

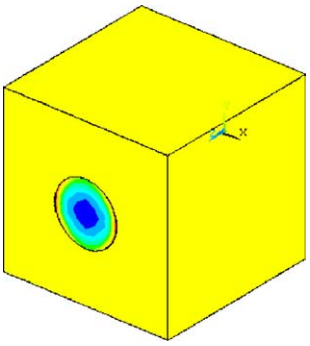

Fig. 30. Electrical displacement distribution D_2.

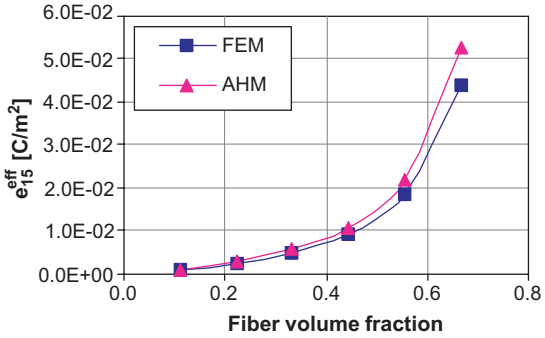

Fig. 31. Variation of e_{15}^{eff} as a function of volume fraction and comparison between FEM and AHM.

6.6. Calculation of ε_{11}^{eff}

$\varepsilon_{11}^{\text{eff}}$ can be evaluated as the ratio of $\overline{D}_2/\overline{E}_2$. In order to solve these equations, all mechanical strains ($\overline{S}_{ij}$) should be made equal to zero. This can be achieved by constraining the displacements at all surfaces to zero. The electric potential difference should be applied in x_1 direction. Then the eighth row of the matrix gives the $\varepsilon_{11}^{\text{eff}}$ coefficient.

Figs. 32 and 33 show the calculated distribution of the electric field $\overline{E}_2$ and the electric displacement $\overline{D}_2$. The variation of this effective coefficient for different volume fractions is shown in Fig. 34.

7. Discussion of results

All 11 effective coefficients have been calculated using AHM and FEM for six different fiber volume fractions. From these discrete fractions graphs were interpolated and shown as comparison between AHM and FEM in the diagrams in Section 6.

The results calculated by AHM were verified by Schulgasser relations and they were fulfilled over the whole range of fiber volume fraction (see Bravo-Castillero et al., 2001). Moreover, the reliability of AHM was proofed in Guinovart-Díaz et al. (2001) and Guinovart-Díaz et al. (2002) where also a com-

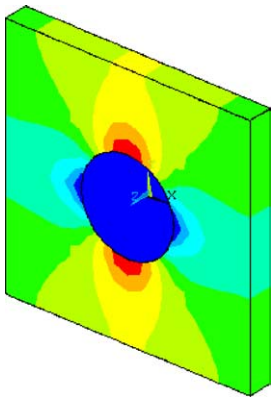

Fig. 32. Strain distribution S_{23}.

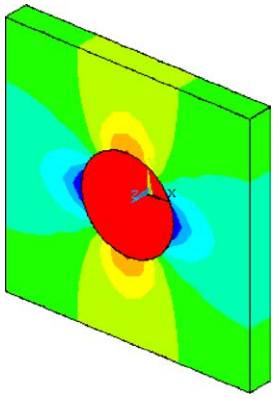

Fig. 33. Electrical displacement distribution D_2.

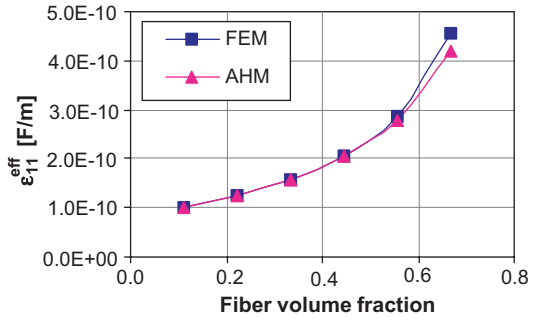

Fig. 34. Variation of $\varepsilon_{11}^{\text{eff}}$ as a function of volume fraction and comparison between FEM and AHM.

parison with irregular in-plane distribution of the fibers was done. There a good concordance has been observed between the models for the calculation of effective coefficients with random distribution and

regular distribution of the fibers using AHM and method of effective field reported in Sevostianov et al. (2001).

The results in this paper show in general a good coincidence between calculation by AHM und FEM. The effective coefficients C_{13}^{eff}, C_{33}^{eff}, e_{13}^{eff}, e_{33}^{eff}, e_{15}^{eff}, $\varepsilon_{11}^{\text{eff}}$, $\varepsilon_{33}^{\text{eff}}$ calculated by FEM show a very good agreement with the coefficients obtained by AHM in all range of the volume fraction. Qualitatively, the behavior of the coefficients C_{11}^{eff}, C_{12}^{eff}, C_{66}^{eff}, C_{44}^{eff} are the same although for a greater value of the volume fraction (0.4 and higher) the curves are not very close. These coefficients are mainly influenced by the in-plane behavior of the composite. Similarly differing results for those coefficients were also stated by other authors (Li and Dunn, 1999; Pettermann and Suresh, 2000). In our opinion the reason lies in the assumed transverse isotropy which is not exactly fulfilled in a square packing because of different fiber distances in diagonal and perpendicular directions. Whereas the analytical method is based strongly on this assumption the numerical method reflect the real fiber arrangement in the finite element model. In a hexagonal fiber arrangement, which is not considered in this paper, the transverse isotropy is really fulfilled. For the practical applications of the calculated effective coefficients these discrepancies must be taken into account.

8. Conclusions

An analytical as well as a numerical approach (RVE) for predicting the homogenized properties of piezoelectric fiber composites has been presented. The numerical approach is based on the finite element method. Longitudinal and transversal elastic and piezoelectric effective coefficients have been calculated with the finite element numerical model and compared with analytical solutions based on the asymptotic homogenization method. This permits us to estimate the range of validity of each approach and to quantify the influence of micro structural parameters, such as the volume fraction, to the effective coefficients. In the case of 1–3 periodic composites with a non-piezoelectric polymer matrix and piezoelectric ceramic (PZT) fibers, the estimation is highly depend on the fiber volume fraction. Both, the unit cell method (RVE) based on the FE as well as analytical methods have their advantages and disadvantages. The analytical approach is able to model statistic distributions and consumes less computing time than the FE analysis. FE analysis on the other hand is appropriate to estimate the effective properties of composites with a given periodic fiber distribution. The FE analysis also allows to include more complex boundary conditions. A generalized approach has been developed to calculate all effective coefficients for all volume fractions by interfacing the finite element package ANSYS with a corresponding FORTRAN routines. It reduces the manual work and time and can be used as a template to determine the effective coefficients of piezoelectric fiber composites with particular arrangement of fibers such as rectangular, hexagonal or random arrangements.

Acknowledgments

This work has been supported by DFG Graduiertenkolleg 828 ''Micro-Macro Interactions in Structured Media and Particle Systems''. Thanks also to the project CITMA, Ciencias Básicas 2004, Cuba. These supports are greatly acknowledged.

References

Bakhvalov, N., Panasenko, G., 1989. Homogenization: Averaging Processes in Periodic Media—mathematical Problems in the Mechanics of Composite Materials. Kluwer, Dordrecht.

Bensoussan, A., Lions, J.L., Papanicolaou, G., 1978. Asymptotic Analysis for Periodic Structures. North-Holland, Amsterdam.

Benveniste, Y., 1992. The determination of elastic and electric fields in a piezoelectric inhomogeneity. J. Appl. Phys. 72 (3), 1086–1095.
Benveniste, Y., 1993. Universal relations in piezoelectric composites with eigenstress and polarization fields. Part I: Binary media—local fields and effective behavior. J. Appl. Mech. 60 (2), 265–269.
Bisegna, P., Luciano, R., 1996. Variational bounds for the overall properties of piezoelectric composites. J. Mech. Phys. Solids 44 (4), 583–602.
Bisegna, P., Luciano, R., 1997. On methods for bounding the overall properties of periodic piezoelectric fibrous composites. J. Mech. Phys. Solids 45 (8), 1329–1356.
Böhm, H.J., 1993. Numerical investigation of microplasticity effects in unidirectional long fiber reinforced metal matrix composites. Modell. Simul. Mater. Sci. Eng. 1 (5), 649–671.
Bravo-Castillero, J., Guinovart-Díaz, R., Sabina, F.J., Rodriguez-Ramos, R., 2001. Closed-form expressions for the effective coefficients of a fiber-reinforced composite with transversely isotropic constituents—II. Piezoelectric and square symmetry. Mech. Mater. 33, 237–248.
Brockenbrough, J.R., Suresh, S., 1990. Plastic deformation of continuous fiber-reinforced metal-matrix composites: effects of fiber shape and distribution. Scr. Metall. Mater. 24, 325–330.
Chan, H.L., Unsworth, J., 1989. Simple model for piezoelectric polymere 1–3 composites used in ultrasonic transducer applications. IEEE Trans. Ultrason. Ferroelectrics Frequency Control 36 (4), 434–441.
Chen, T., 1993. Piezoelectric properties of multiphase fibrous composites: some theoretical results. J. Mech. Phys. Sol. 41 (11), 1781–1794.
Cleveringa, H.H.M, van der Giessen, E., Needleman, A., 1997. Comparison of discrete dislocations and continuum plasticity predictions for a composite material. Acta Metall. Mater. 45 (8), 3163–3179.
Dunn, M.L., Taya, M., 1993. Micromechanics predictions of the effective electroelastic moduli of piezoelectric composites. Int. J. Sol. Struct. 30 (2), 161–175.
Dunn, M.L., Wienecke, H.A., 1997. Inclusions and inhomogeneities in transversely isotropic piezoelectric solids. Int. J. Sol. Struct. 34 (27), 3571–3582.
Gaudenzi, P., 1997. On the electromechanical response of active composite materials with piezoelectric inclusions. Comput. Struct. 65 (2), 157–168.
Guinovart-Díaz, R., Bravo-Castillero, J., Rodríguez-Ramos, R., Sabina, F.J., Martínez-Rosado, R., 2001. Overall properties of piezocomposite materials 1–3. Mater. Lett. 48, 93–98.
Guinovart-Díaz, R., Bravo-Castillero, J., Rodríguez-Ramos, R., Martínez-Rosado, R., Serranía, F., Navarrete, M., 2002. Modeling of elastic transversely isotropic composite using the asymptotic homogenization method. Some comparisons with other models. Mater. Lett. 56, 889–894.
Gunawardena, S.R., Jansson, S., Leckie, A., 1993. Modeling of anisotropic behavior of weakly bonded fiber reinforced MMCs. Acta Metall. Mater. 41 (11), 3147–3156.
Levin, V.M., Rakovskaja, M.I., Kreher, W.S., 1999. The effective thermoelectroelastic properties of microinhomogeneous materials. Int. J. Sol. Struct. 36, 2683–2705.
Li, J.Y., Dunn, M.L., 1999. Analysis of micro structural fields in heterogeneous piezoelectric solids. Int. J. Eng. Sci. 37, 665–685.
Meguid, S.A., Kalamkarov, A.L., 1994. Asymptotic homogenization of elastic composite materials with a regular structure. Int. J. Sol. Struct. 31, 303–316.
Pettermann, H.E., Suresh, S., 2000. A comprehensive unit cell model: a study of coupled effects in piezoelectric 1–3 composites. Int. J. Sol. Struct. 37, 5447–5464.
Pobedria, B.E., 1984. Mechanics of Composite Materials. Moscow State University Press, Moscow (in Russian).
Poizat, C., Sester, M., 1999. Effective properties of Composites with Embedded piezoelectric fibers. Comput. Mater. Sci. 16, 89–97.
Reisner, G., Werner, E.A., Fischer, F.D., 1998. Micromechanical modeling of martesitic transformation in random microstructures. Int. J. Sol. Struct. 35 (19), 2457–2473.
Rodriguez-Ramos, R., Guinovart-Díaz, R., Sabina, F.J., Bravo-Castillero, J., 2001. Closed-form expressions for the effective coefficients of fiber-reinforced composite with transversely isotropic constituents – I. Elastic and square symmetry. Mech. Mater. 33, 223–235.
Sevostianov, I., Levin, V., Kachanov, M., 2001. On the modeling and design of piezocomposites with prescribed properties. Arch. Appl. Mech. 71, 733–747.
Silva, E.C.N., Fonseca, J.S.O., Kikuchi, N., 1998. Optimal design of periodic piezocomposites. Comput. Methods Appl. Eng. 159, 49–77.
Smith, W.A., Auld, B.A., 1991. Modelling 1–3 composite piezoelectrics: thickness-mode oscillations. IEEE Trans. Ultrason. Ferroelectrics Frequency Control 38 (1), 40–47.
Smith, R.J.M., Brekelmans, W.A.M., Meijer, H.E.H., 1998. Prediction of the mechanical behavior of nonlinear heterogeneous systems by multi-level finite element modeling. Comput. Methods Appl. Eng. 155, 181–192.
Suquet, P., 1987. Elements of homogenization theory for inelastic solid mechanics. In: Sanchez-Palencia, E., Zaoui, A. (Eds.), Homogenization Techniques for Composite Media. Springer-Verlag, Berlin, pp. 194–275.

Teply, J.L., Dvorak, G.J., 1988. Bounds on overall instantaneous properties of elastic–plastic composites. J. Mech. Phys. Solids 36 (1), 29–58.
Wang, B., 1992. Three-dimensional analysis of an ellipsoidal inclusion in a piezoelectric material. Int. J. Sol. Struct. 29, 293–308.